# BRDF Measurement of Highly-Specular Materials using a Goniometer

Jiří Filip[a], Radomír Vávra[a], Frank J. Maile[b]

[a] *Institute of Information Theory and Automation of the CAS, Praha, Czech Republic*
[b] *Schlenk Metallic Pigments GmbH, Roth-Barnsdorf, Germany*

**Abstract**

Visually accurate capture of appearance of highly specular surfaces is of a great research interest of the coating industry, who strive to introduce highly reflective products while minimizing their production and quality assessment costs, and avoiding environmental issues related to the production process. An efficient measurement of such surfaces is challenging due to their narrow specular peak of an unknown shape and typically very high dynamic range. Such behavior puts higher requirements on capabilities of a measuring device and has impact on length of the measurement process. In this paper, we rely on a material probes with a predefined curved shape featuring slight local inhomogeneities. This defines a goniometric device as appropriate means of appearance capture. To shorten a typically long measurement time required when using these approaches, we introduce a method of material appearance acquisition by means of the isotropic BRDF using relatively sparse sampling adapted to each measured material individually.

*Keywords:* BRDF, gloss, material, specular, goniometer, adaptive, measurement, chrome-like appearance, high-reflective, mirror-like coatings

## 1. Introduction

The understanding of principles defining the human perception of highly reflective mirror-like surfaces is one of the major research challenges of computer graphics. In particular, the visually accurate measurement and reproduction of such surfaces is of a vital research interest to coating industry striving to introduce highly reflective products that could substitute the appearance of more expensive natural materials while minimizing production and quality control costs. Also, there is no optical *standard* established which complicates *color* communication in this industry in general. Electroplated chrome surfaces are chosen as a reference, but their manufacturing is under pressure due to environmental reasons as the process uses harmful $Cr^{6+}$ which causes cancer [1]. For this reason, the complete industry is looking for chrome replacements in order to match as close as possible the appearance of this chrome-like look. Here, one possibility is the use of coatings incl. metallic pigments especially vacuum metallic pigments (VMP) [2].

Results shown in this paper are part of a wider research project analyzing human perception of highly specular or glossy surfaces. Our past experiments revealed that different shapes covered by the same specular material induce different perceptions of gloss (see Fig. 1). Therefore, an ultimate goal is the identification of links between subjective visual perception and objective computational measures and their interaction with surface shape, unifying and simplifying the communication of the highly-specular material appearance at both academic and industrial levels.

For the sake of this project, a specific curved surface shape is selected as shown in Fig. 2, in order to be easily manipulated and evaluated by human subjects. As exactly the same samples should be used for surface appearance measurement

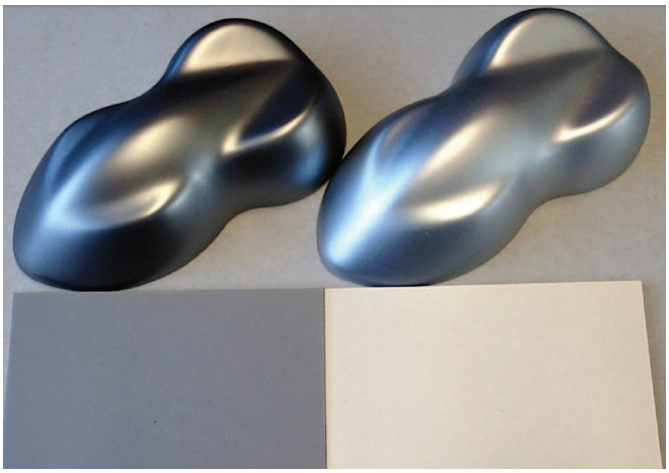

Figure 1: Influence of 3D object shape on overall visual perception of highly-reflective coatings including VMPs [2]. Identical coatings sprayed on black (left) and white (right) panels and speedshapes.

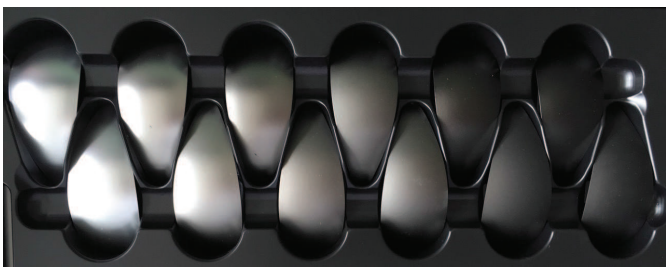

Figure 2: Examples of physical samples used for subjective assessment and objective measurement of reflective materials. Samples courtesy of Lechler S.p.a. Como, Italy.

and its further subjective evaluation, we cannot prepare proprietary flat, cylindrical, or spherical samples which are more suitable for image-based appearance capture systems. Although the selected shape is great for the subject, for the assessment of specular properties, it puts higher demands on the measurement process. Additionally, due to possible local spatial inhomogeneity of the curved sample, only a small area is selected for effective measurement. These requirements, together with the nature of specular materials, i.e., narrow specular peaks of a high dynamic range, resulted in an appearance measurement using a sequential goniometric sampling.

This paper focuses specifically on the measurement of material appearance by an isotropic Bidirectional Reflectance Distribution Function (BRDF). However, sequential measurement of the BRDF using goniometers is typically very slow, so the main contribution of this paper is an introduction of a data-driven measurement method that adapts the sampling steps particularly along specular highlights in accordance with reflective properties of measured materials. This allows for the relatively sparse measurement of the BRDF in a reasonable time-frame, even using a relatively slow measurement process. We also thoroughly discuss many practical issues related to the goniometric appearance measurement of highly specular materials.

Our paper is structured as follows. Section 2 introduces the related work. Section 3 describes the theoretical background of BRDF representation, while Section 4 describes the measurement device, material probes and other practical issues. Section 5 outlines the proposed adaptive method of BRDF measurement, whose results are visually compared with other similar public specular BRDF data in Section 6. Section 7 concludes the paper.

## 2. Related Work

Our paper is related to BRDF parameterization methods and their respective measurement approaches.

**Parameterization of BRDF data** holds a key importance in development of efficient acquisition and rendering algorithms. Depending on the required priority, the data can be organized in a way more suitable to certain compression [3] or importance sampling [4] methods. Different parameterizations suggested for several analytical BRDF models are studied in [5]. In this work, we focus ourselves on the half-difference BRDF parameterization [3]. Although this parametrization is inherently anisotropic, it is typically used to represent isotropic materials only.

**Anisotropic BRDF measurement methods** can be split into two groups based on their ability to record material anisotropy or not. However, as a dense measurement of the anisotropic BRDF using gonioreflectometers [6, 7, 8, 9] is very time demanding, setups were developed that reduced the required number of mechanical degrees-of-freedom (DOF). Many setups use mirrors, e.g., spherical mirror [10], kaleidoscopically arranged flat mirrors [11], parabolic mirrors [12], ellipsoidal mirrors [13], or a combination of concave parabolic and custom-built mirrors [14]. They allowed for the capture of many viewing directions simultaneously; however, a limited range of elevation angles resulted. Other methods used setups consisting of multiple light sources and sensors [15, 16], which shorten the measurement time significantly at the cost of a fixed measurement geometry. Another group of acquisition methods reduces the number of DOF by using a specimen of a known shape (e.g., spherical, cylindrical or flat). These setups capture either isotropic [17] or anisotropic [18, 19, 20] BRDF data. However, accuracy of these measurements is often compromised due to slight inhomogeneity of a specimen and its shape imperfections. A notable source of public isotropic BRDFs of several highly specular samples is the MERL BRDF database [17].

In this paper, we focus on the measurement of the isotropic BRDF of highly specular materials using an image-based goniometer, i.e., using a camera to capture the reflected radiance intensity.

## 3. Theoretical Background

Real-world appearance of spatially homogeneous materials can be represented by means of the BRDF as introduced by Nicodemus et al. [21]. It is a four-dimensional vector-valued function $f_r(\theta_i, \theta_v, \varphi_i, \varphi_v)$ of the illumination direction $\omega_i = \{\theta_i, \varphi_i\}$ and the viewing direction $\omega_v = \{\theta_v, \varphi_v\}$ that defines how light is reflected at the surface of a material and where $\theta \in [0, \frac{\pi}{2}]$ is the elevation angle and $\varphi \in [0, 2\pi)$ is the azimuthal angle of a spherical coordinate system.

The general four-dimensional function can describe anisotropic materials, i.e., those that have variable reflectance when they are rotated along a surface normal. This property is common for many real-world materials that contain directional elements such as thread in fabric or grain in wood. A three-dimensional simplification of the BRDF is called the isotropic BRDF $f_r(\theta_i, \theta_v, \Delta\varphi = \varphi_v - \varphi_i)$ and it neglects anisotropic appearance.

The main limitation of the standard parameterization, which is shown in Fig. 3-a, is its inefficient representation of important features, such as specular highlights not aligned with axes of the coordinate system. Therefore, locations of the highlights depend on several variables and usage of standard parameterization for, e.g., compression of the BRDF, is limited.

These limitations are leveraged by the half-difference (HD) parameterization proposed by Rusinkiewicz [3]. He changes variables from $f_r(\theta_i, \varphi_i, \theta_v, \varphi_v)$ to $f_r(\theta_h, \varphi_h, \theta_d, \varphi_d)$ as show in Fig. 3-b. The BRDF is represented by the half vector $\mathbf{H} = \{\theta_h, \varphi_h\}$ between the illumination and viewing directions, and by the difference vector $\mathbf{D} = \{\theta_d, \varphi_d\}$, which represents the illumination direction $\mathbf{I}$ with respect to the half vector $\mathbf{H}$.

The HD parametrization is, due to its effective description of specular highlights, widely used in analytical BRDF models, e.g., [10], [22]. The shape of specular highlights is represented by the elevation angle of the half vector $\theta_h$, and the ideal mirror reflection is obtained for $\theta_h = 0°$, i.e., when the half vector is aligned with the normal of the surface. A non-linear sampling along $\theta_h$ is often used to reproduce a highly specular material with a limited number of samples [17]. Anisotropic behavior

is controlled by the azimuthal angle of the half vector $\varphi_h$ as represented by the rotation of a sample around its normal.

On the other hand, a value of the elevation angle of the difference vector $\theta_d$ is equal to one half of the angle between a camera and a light source. Therefore, at $\theta_d = 0°$ are ideal retro-reflections. Reciprocity is introduced by symmetry of the azimuthal angle of the difference vector $\varphi_d = \varphi_d + c\pi$, where $c \in \mathbb{Z}$. Therefore, a range of the angles is $\theta_h, \theta_d \in [0, \frac{\pi}{2}], \varphi_h \in [0, 2\pi), \varphi_d \in [0, \pi)$. The isotropic BRDF can be described by its three-dimensional variant $f_r(\theta_h, \theta_d, \varphi_d)$ by omitting dependence on azimuth $\varphi_h$.

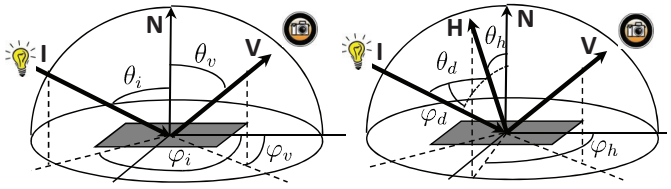


(a) (b)

Figure 3: BRDF parameterizations: (a) spherical, (b) half-difference.

## 4. BRDF Measurement

In this section, we first introduce a BRDF acquisition device and material probes we use for experiments. Next, we discuss general practical issues we dealt with over the measurement process.

### *4.1. Acquisition Device*

We use the UTIA gonioreflectometer [8] to capture appearance of the tested coatings (see Sec. 4.2). This state-of-the-art setup (see Fig. 4) consists of a rotary stage, holding a measured sample and two independently controlled arms with a camera (one axis) and a light source (two axes). It allows a flexible,

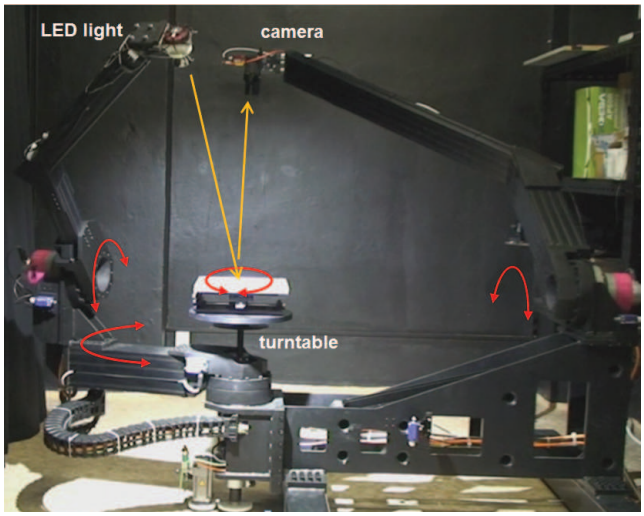


Figure 4: The UTIA gonioreflectometer.

adaptive measurement of a nearly-arbitrary combination of illumination and viewing directions. Although an occlusion of view of the camera by the arm with the light source may occur, it can be analytically detected and, in the most cases, an alternative positioning of the arms exists. Verified angular accuracy of positioning of the arms across all axes is 0.03 degree. The inner arm holds a LED light source 1.1 m far from a sample, which produces a narrow and uniform beam of light. The outer arm holds an industrial full-frame 16 Mpix RGB camera AVT Pike 1600C. The distance of the sensor from a sample is 2 m. When we use different optics, we can achieve an arbitrary spatial resolution up to 1071 DPI (i.e., 24 $\mu$m/pixel). In our experiment, we used a resolution of 353 DPI (i.e., 70 $\mu$m/pixel). We perform color calibration of the camera using the X-Rite Color Checker target.

### *4.2. Material Probes*

We measure two highly-specular materials: a green paint with a thick layer of acrylic coating and casted silver 925 mechanically polished to maximal surface smoothness as shown in Fig. 5. As our work is related to other studies that analyze human visual perception of highly reflective materials, the samples feature rounded shapes. The samples were kindly provided by the Lechler S.p.a. Como, Italy refinishing-paint company. Since the rounded shape poses problems due to the repeated attachment of a sample to the measuring device and its precise geometrical alignment owing to the coordinate system of the device, we designed a proprietary holder mounted on an x-y-z linear positioning stage. As only a small area of 3×3 mm on the top of the sample is used for data collection, its normal should be aligned with the normal of the turntable. The alignment of a sample is adjusted and verified by iterative adjustment of its position, while we test stationarity of the specular highlight position for several rotations of the turntable.

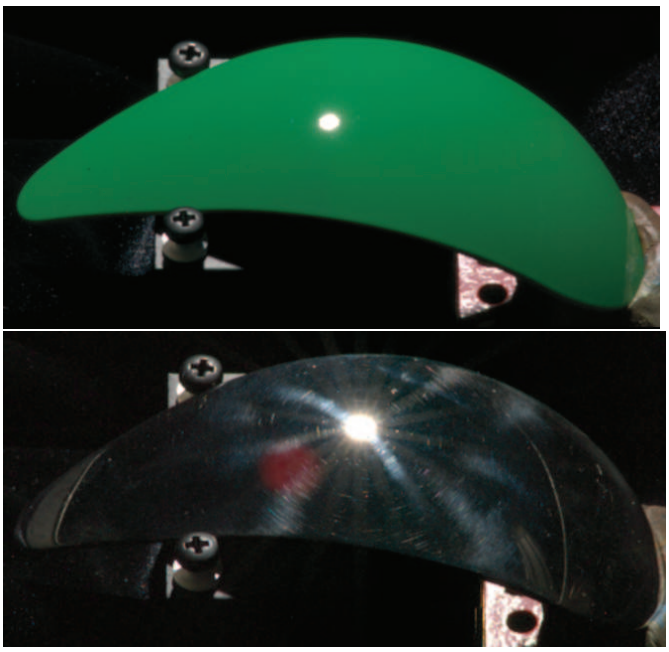

Figure 5: Two measured specular materials: (top) the green paint with acrylic coating and (bottom) the highly polished silver 925. Sample shape courtesy of Lechler S.p.a. Como, Italy

### 4.3. Measurement Related Issues

Measurement of highly specular materials is tricky due to several visual artifacts related to high reflectivity and thus a high dynamic range of the measured material. Most of the artifacts are, due to its reflectivity, present only for the silver sample. Their overview is given in Fig. 6 and they are discussed in more detail in this section.

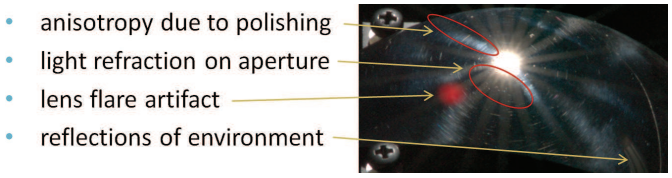


Figure 6: Challenges encountered during measurement of the highly specular material.

**Anisotropic artifacts** – originate from insufficient smoothness of the otherwise isotropic material. Such material often exhibits local microscopic scratches, which are visible when illumination and viewing directions are perpendicular to the direction of scratches (see Fig. 6). A correct appearance of scratches cannot be captured by the isotropic half-difference parameterization, and they result in anisotropic artifacts within the rendering. Examples of such artifacts for *steel* and *chrome-steel* materials from the MERL database [17] are shown in Fig. 7-a,b, and in Fig. 7-c for our measurement of silver. These artifacts can be

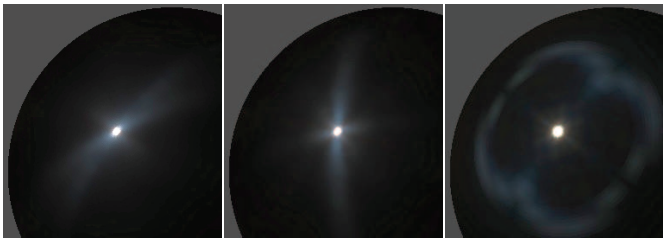

(a) *steel* (b) *chrome-steel* (c) *silver 925*

Figure 7: Anisotropic artifacts in the captured isotropic BRDF: (a) *steel*, and (b) *chrome-steel* from the MERL database, and (c) silver from our measurement.

often avoided by selecting a proper value of the $\varphi_h$ parameter, i.e., by an appropriate initial orientation of a sample before a measurement process. We use this solution to remove artifacts.

**Lens flare** – occurs in the presence of a strong light source in a scene. This phenomenon is caused by an internal reflection and scattering within the body of a lens, and is more pronounced for lenses with a large number of elements. For our fixed lens, it exhibits itself merely as a bright red spot (see Fig. 6). This artifact can be, to a certain extent, eliminated by using a sufficiently long cylindrical lens hood or by applying an appropriate photographic filter. The latter might, however, impact other aspects of measured appearance; therefore, we have carefully checked all captured images for the presence of local color changes so as to avoid contamination of measured data by this artifact.

**Diffraction on an aperture** – occurs due to the wave nature of light. When distant bright light passes through a narrow slit, it causes that the light spreads perpendicularly to the slit. Usage of a small aperture creates a slit-like situation at the corners of the blades of the aperture. This effect is more pronounced for narrow apertures and bright point-like illumination. The resulting bright streaks in a star-like shape influence measured BRDF values in an unpredictable manner when the specular highlight approaches the sampled area. Therefore, as a counter measure, we replaced the original aperture in a lens by a circular one of a similar diameter. The results of this step are satisfactory as shown in Fig. 8. The diffraction effect is more intensive the

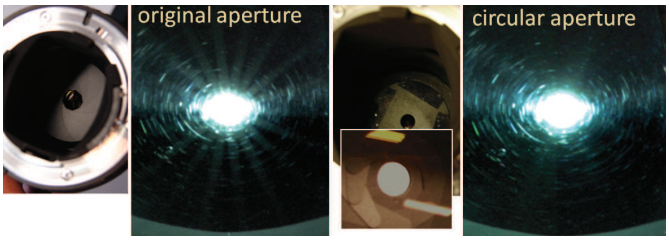


Figure 8: Diffraction on the aperture of a lens (left), and its suppression by usage of the circular aperture (right).

narrower the light source as shown in Fig. 9, which compares two light sources having different emitting areas.

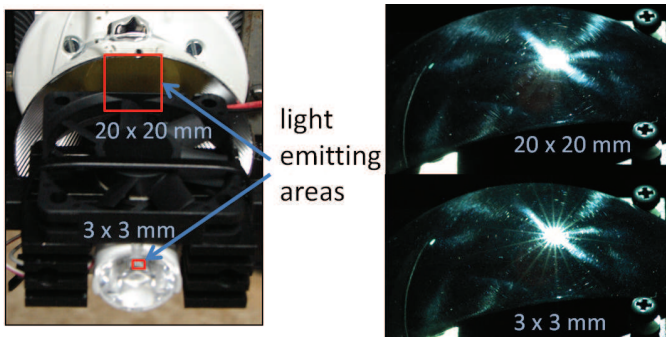


Figure 9: Impact of the size of the area that emits light on diffraction level.

**Reflections from environment** – are naturally present when a specular material is measured. They can be suppressed by using diffuse black materials for all components surrounding the measured sample.

## 5. Proposed Measurement Approach

The proposed measurement process can sample even a highly specular isotropic material with a very limited number of samples. Specifically, we place samples along $\theta_d$ with a step of 3°, along $\varphi_d$ with a step of 15° and we place 30 samples along $\theta_h$ non-linearly. It results into $|\theta_h| \times |\theta_d| \times |\varphi_d| = 30 \times 30 \times 7 = 6300$ samples which can be measured by the goniometer in reasonable time. The measurement process can be divided into two steps. The first one estimates the optimal parameter of a non-linear distribution of samples along a specular highlight ($\theta_h$), while the second part realizes the sparse BRDF measurement

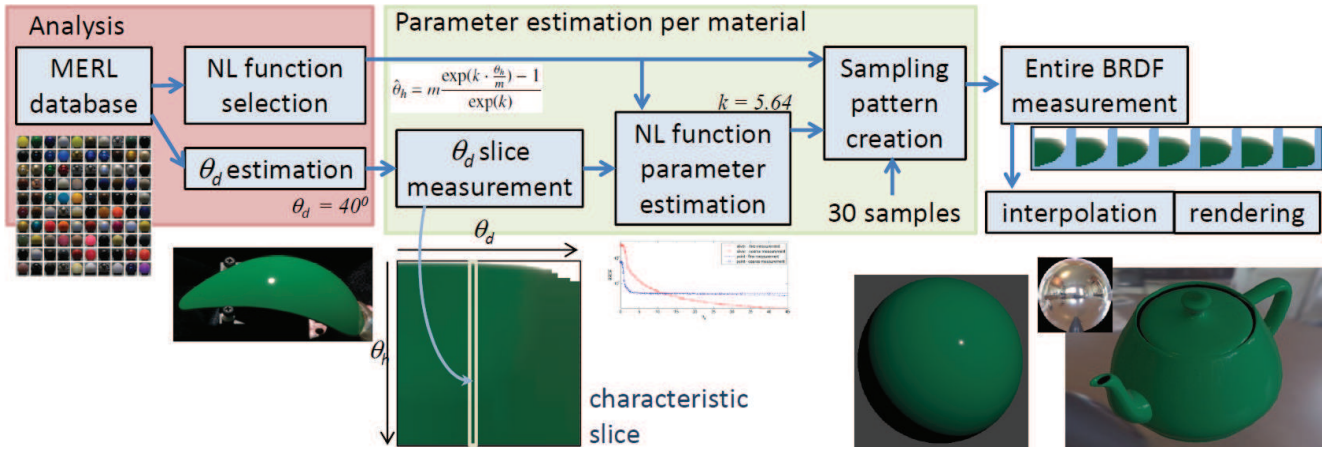


Figure 10: An overview of the analysis prior to the measurement, estimation of the parameter, and preparation of sparse sampling during the measurement of a new material.

using the parameter obtained in the previous step. The estimation of the optimal parameter is performed by a fine measurement of a single slice of variable $\theta_h$ for other parameters constant and by computation of its value enabling the best approximation of measured data.

Prior to any measurement of a new material, we performed analysis of already measured materials in the MERL database. The analysis serves for determining the optimal function of the non-linear distribution of samples, whose parameter is then estimated for each new measured material. It also decides the optimal position of a slice, whose values are measured for further estimation of the parameter. An overview of the analysis and the entire measurement process is given in Fig. 10.

### 5.1. Analysis of the MERL database

Once we want to sample a highly specular material using the limited number of samples, one of the most challenging tasks is a proper non-linear sampling along $\theta_h$, where the reflected intensity changes in orders of magnitude within a fraction of a degree. This is clearly shown in an example of the characteristic slice ($\theta_h \times \theta_d$) of *steel* from the MERL database [17] in Fig. 11. On the left side, one can observe a very sharp transition between specular and off-specular values when the $\theta_h$ is sampled linearly. Therefore, non-linear sampling of $\theta_h$ using the square root is often applied (1) as shown on the right side.

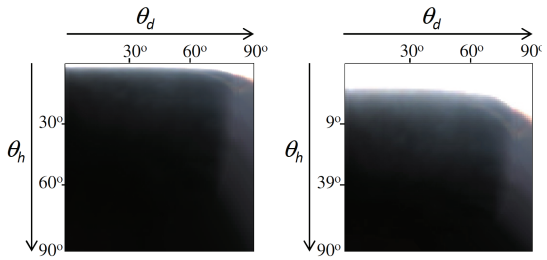


Figure 11: The characteristic slice of the BRDF (dependency on $\theta_h, \theta_d$) of highly-specular material: (left) the linear sampling along $\theta_h$, (right) the non-linear sampling along $\theta_h$ using square root (1).

However, application of the square root (1) is not always the best choice when we want to sample a material sparsely; therefore, our analysis is focused on identifying an appropriate non-linear function, whose parameter might be adapted to a measured material enabling the precise capturing of the dynamic shape of specular reflection along $\theta_h$ using the very limited number of samples.

To identify a proper sampling along $\theta_h$, we have to select an appropriate fixed value of $\theta_d$, i.e., choose a column of a characteristic slice as measured in the first step of the process. To this end, we use BRDFs from the MERL database as training data. To determine the non-linear sampling function that performs the best and the optimal value of $\theta_d$, we tested three functions (see (2), (3), (4)) that distribute samples along $\theta_h$ non-linearly.

$$\hat{\theta}_h = \frac{\theta_h^2}{90^\circ} \tag{1}$$

$$\hat{\theta}_h = m\left(\frac{\theta_h}{m}\right)^k, \quad k > 0 \tag{2}$$

$$\hat{\theta}_h = m\frac{\exp(k\cdot\frac{\theta_h}{m})-1}{\exp(k)-1}, \quad k > 0 \tag{3}$$

$$\hat{\theta}_h = m\frac{k^{\frac{\theta_h}{m}}-1}{k-1}, \quad k > 1 \tag{4}$$

Notice the square root mapping used in the MERL database (1) is the special case of (2) for $k = 2$. The parameter $m$ is the maximal possible value of $\theta_h$. A comparison of the square root mapping (red dashed) with the other tested functions for parameter $k = 4$ is given in Fig. 12.

We focus our analysis on a single characteristic slice for $\varphi_d = 90^\circ$ that holds the most descriptive information on the BRDF. Over all 100 BRDFs, we try to identify the function (2, 3, 4) and the value of $\theta_d$, thus enabling on average, the best approximation of the characteristic slice based on a sparse non-linear measurement whose parameter $k$ is estimated from the detailed measurement of the single column. Specifically, we

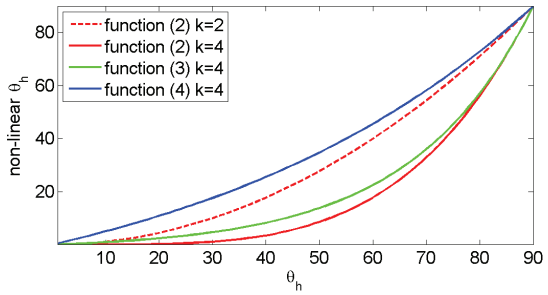


Figure 12: A comparison of the functions tested for non-linear mapping of $\theta_h$.

compute a mean absolute error between the original characteristic slice and its reinterpolated variant. Finally, we identified that function (3) in combination with $\theta_d = 40°$ works the best.

### 5.2. Material-Driven Sampling Pattern Adaptation

Once we have a fixed elevation $\theta_d = 40°$ and a non-linear function (3), we can apply this information to an efficient measurement of an unknown specular material. First, we initially rotate the material to appropriate $\varphi_h$ so as to avoid anisotropic artifacts. Then for $\varphi_d = 90°$ and $\theta_d = 40°$, we capture BRDF values by way of up to 90 samples distributed along $\theta_h$ using standard square root non-linear sampling. Next, we estimate parameter $k$ of the function (3) to find its optimal value $\hat{k}$, that fits the measured data the best.

Finally, given the required number of samples, we prepare the sparse sampling pattern along $\theta_h$, using the optimal parameter $\hat{k}$ and the function (3) and perform the measurement. The estimated value of parameter $\hat{k}$ for the paint is 5.64 and for the silver is 4.78.

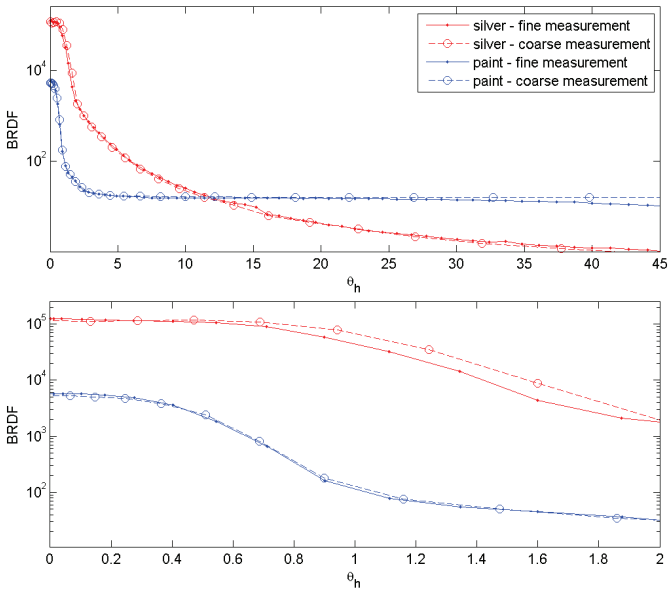


Figure 13: A comparison of intensity captured for two tested materials by means of a standard squared root non-linear mapping using up to 90 samples along $\theta_h$ (solid line), compared to proposed adaptive non-linear mapping using up to 30 samples along $\theta_h$ (dashed line). The other parameters are fixed at $\varphi_h = 45°, \theta_d = 40°, \varphi_d = 90°$. The second graph shows in more detail a surrounding of the specular highlight $\theta_h = 0$ - $2°$.

A graph in Fig. 13 compares BRDF data for fixed $\varphi_h = 45°, \theta_d = 40°, \varphi_d = 90°$ using the fine initial sampling along $\theta_h$ with up to 90 samples (shown as solid line), with the BRDF data obtained by the proposed adaptive sampling using up to 30 samples (shown as dashed line). One can observe a very close resemblance of values for both tested materials, especially near the specular highlight (see a detail in the bottom graph).

### 5.3. Sparse BRDF measurement

The measurement process using a goniometric device is long due to sequential sampling of bidirectional pairs. To eliminate the number of taken samples, we suggest the following. We capture elevation angles by 30 samples each, while sampling along $\theta_d$ is linear with step 3°, sampling along $\theta_h$ is non-linear using the pattern derived by the method above. As the appearance of the characteristic slice is symmetrical around $\varphi_d = 90°$, we capture $\varphi_d$ only in interval $(0° - 90°)$ and replicate it to interval $(180° - 90°)$. Due to small differences between characteristic slices along $\varphi_d$, we capture only seven of them with the linear sampling step of 15°. Azimuthal angle of the half direction is fixed at $\varphi_h = 45°$ to avoid anisotropic artifacts. Therefore, the theoretical number of samples is $|\theta_h| \times |\theta_d| \times |\varphi_d| = 30 \times 30 \times 7 = 6300$ samples. However, due to limitations of the measuring device (i.e., $\theta_v \leq 75°$), the number of measured samples is 4073 in total. To capture these samples in a high dynamic range, multiple exposures and intensities of light are used, resulting in a measurement time of 15 hours.

Fig. 14 shows a captured BRDF with the contribution of anisotropic artifacts and a reddish hue due to the diffraction on the aperture of variable size (a) and (b), and the final BRDF with the artifacts compensated for (c).

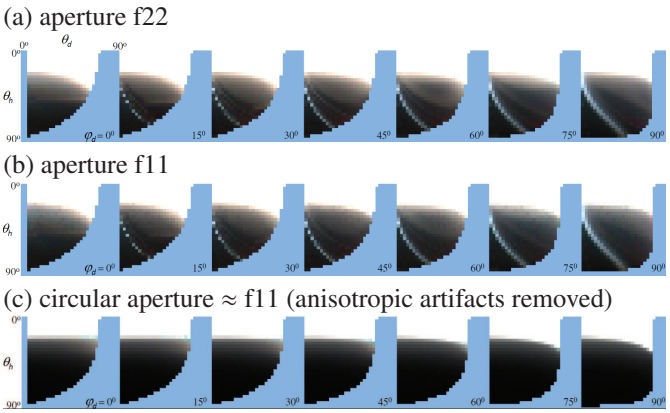


Figure 14: Measured BRDF of the silver 925: (a) aperture f22, (b) aperture f11, (c) circular aperture ≈f11.

Finally, non-measured values shown as blue (due to a camera/light occlusion or low elevations) are extrapolated from measured values, and resulting data are linearly interpolated into the sampling format of the MERL database, i.e., in a resolution of $|\theta_h| \times |\theta_d| \times |\varphi_d| = 90 \times 90 \times 180 = 1458000$ samples. Such a dataset is eventually used for BRDF rendering in the following section.

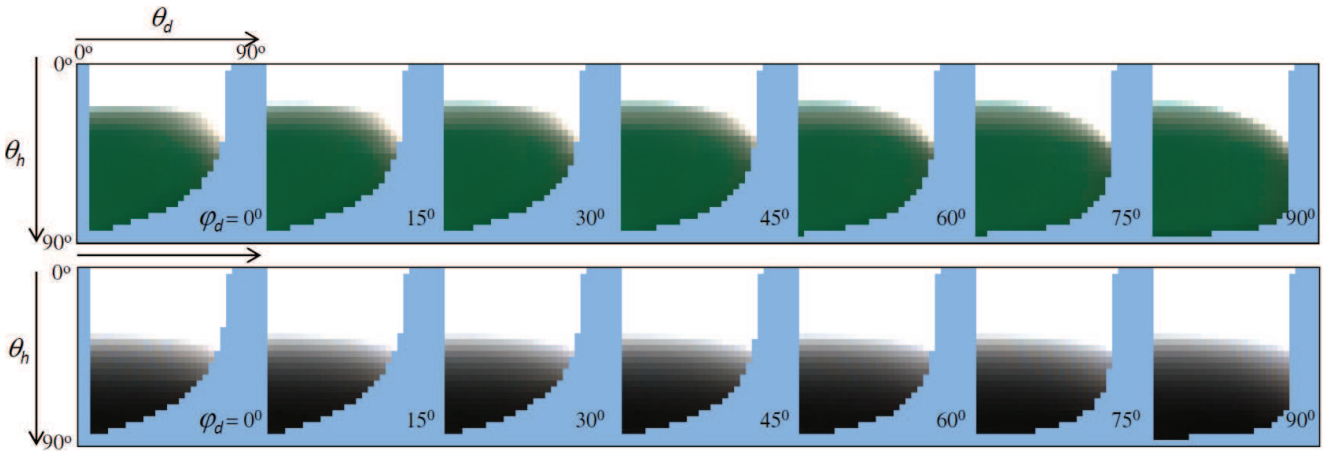


Figure 15: Visualization of captured raw samples used for BRDF reconstruction. The first row is paint, the second row is silver 925. Non-measured blue areas are further extrapolated.

## 6. Results

All raw BRDF samples captured by the goniometer for both measured materials are illustrated in Fig. 15 as a consecutive sequence of characteristic slices.

Note, the wider width of specular highlight of the silver sample as compared to the paint sample. Similarly, the silver sample has, in order of magnitude higher dynamic range as shown in Fig. 13.

Ray-tracings in PBRT2 of the measured BRDFs compared to the most similar materials from the MERL BRDF database are shown in Fig. 16. Similar results on a speedshape object in a Mitsuba renderer are given in Fig. 17. In general, one can observe a higher intensity of reflection from silver when compared to *steel* and *chrome* materials. On the other hand, *steel* and *chrome* feature sharper reflections presumably due to the electrostatic plating surface finish as compared to mechanical polishing of the casted silver probe.

## 7. Conclusion

In this paper, we focused on the isotropic BRDF measurement of highly specular materials using a gonioreflectometer. We discussed challenges encountered during the measurement of such materials and proposed a novel approach to an efficient BRDF capturing of highly specular materials using a data-driven adaptive sampling of specular highlights. This approach allows us to considerably reduce the required measurement time while still maintaining a high accuracy of measured data. We tested our method by the capturing of a paint with an acrylic clear coat and a casted, polished silver sample. Finally, we compared our results with other state-of-the-art BRDF measurements of similar materials.

## Acknowledgments

This research has been supported by the Czech Science Foundation grant GA17-18407S.

## References

[1] Maile, F.J., Martins, A.C.. Chrome-like effects without chromium. Pitture e Vernici 2015;(1):16–22.

[2] Maile, F.J., Pfaff, G., Reynders, P.. Effect pigments: past, present and future. Progress in organic coatings 2005;54(3):150–163.

[3] Rusinkiewicz, S.. A new change of variables for efficient BRDF representation. In: Rendering techniques' 98. 1998, p. 11–22.

[4] Havran, V., Filip, J., Myszkowski, K.. Bidirectional texture function compression based on the multilevel vector quantization. Computer Graphics Forum 2010;29(1):175–190.

[5] Stark, M., Arvo, J., Smits, B.. Barycentric parameterizations for isotropic BRDFs. IEEE TVCG 2005;11(2):126 –138.

[6] Murray-Coleman, J., Smith, A.. The automated measurement of BRDFs and their application to luminaire modeling. Journal of the Illuminating Engineering Society 1990;19:87–99.

[7] Holroyd, M., Lawrence, J., Zickler, T.. A coaxial optical scanner for synchronous acquisition of 3D geometry and surface reflectance. ACM Trans Graph 2010;29:99:1–99:12.

[8] Filip, J., Vavra, R., Haindl, M., Zid, P., Krupicka, M., Havran, V.. BRDF slices: Accurate adaptive anisotropic appearance acquisition. In: CVPR. 2013, p. 4321–4326.

[9] Höpe, A., Atamas, T., Hünerhoff, D., Teichert, S., Hauer, K.O.. Argon$^3$: 3D appearance robot-based gonioreflectometer at PTB. Review of Scientific Instr 2012;83(4).

[10] Ward, G.. Measuring and modeling anisotropic reflection. Computer Graphics 1992;26(2):265 – 272.

[11] Han, J., Perlin, K.. Measuring bidirectional texture reflectance with a kaleidoscope. ACM SIGGRAPH 2003 2003;22(3):741–748.

[12] Dana, K., Wang, J.. Device for convenient measurement of spatially varying bidirectional reflectance. Journal of Optical Society of America 2004;21(1):1–12.

[13] Mukaigawa, Y., Sumino, K., Yagi, Y.. Rapid BRDF measurement using an ellipsoidal mirror and a projector. IPSJ Trans on Computer Vision and Appl 2009;1:21–32.

[14] Ghosh, A., Heidrich, W., Achutha, S., OToole, M.. A basis illumination approach to BRDF measurement. International Journal of Computer Vision 2010;90(2):183–197.

[15] Ben-Ezra, M., Wang, J., Wilburn, B., Li, X., Ma, L.. An LED-only BRDF measurement device. Computer Vision and Pattern Recognition, IEEE Computer Society Conference on 2008;0:1–8.

[16] Schwartz, C., Sarlette, R., Weinmann, M., Klein, R.. DOME II: A parallelized BTF acquisition system. In: Rushmeier, H., Klein, R., editors. Eurographics Workshop on Material Appearance Modeling: Issues and Acquisition. Eurographics Association; 2013, p. 25–31.

[17] Matusik, W., Pfister, H., Brand, M., McMillan, L.. A data-driven reflectance model. ACM Transactions on Graphics 2003;22(3):759–769.

[18] Lu, J., Little, J.. Reflectance function estimation and shape recovery from image sequence of a rotating object. In: Proceedings of the Fifth


Figure 16: A comparison of ray-tracing of captured BRDFs of paint and silver with similar materials from the MERL BRDF database using a PBRT2 renderer.

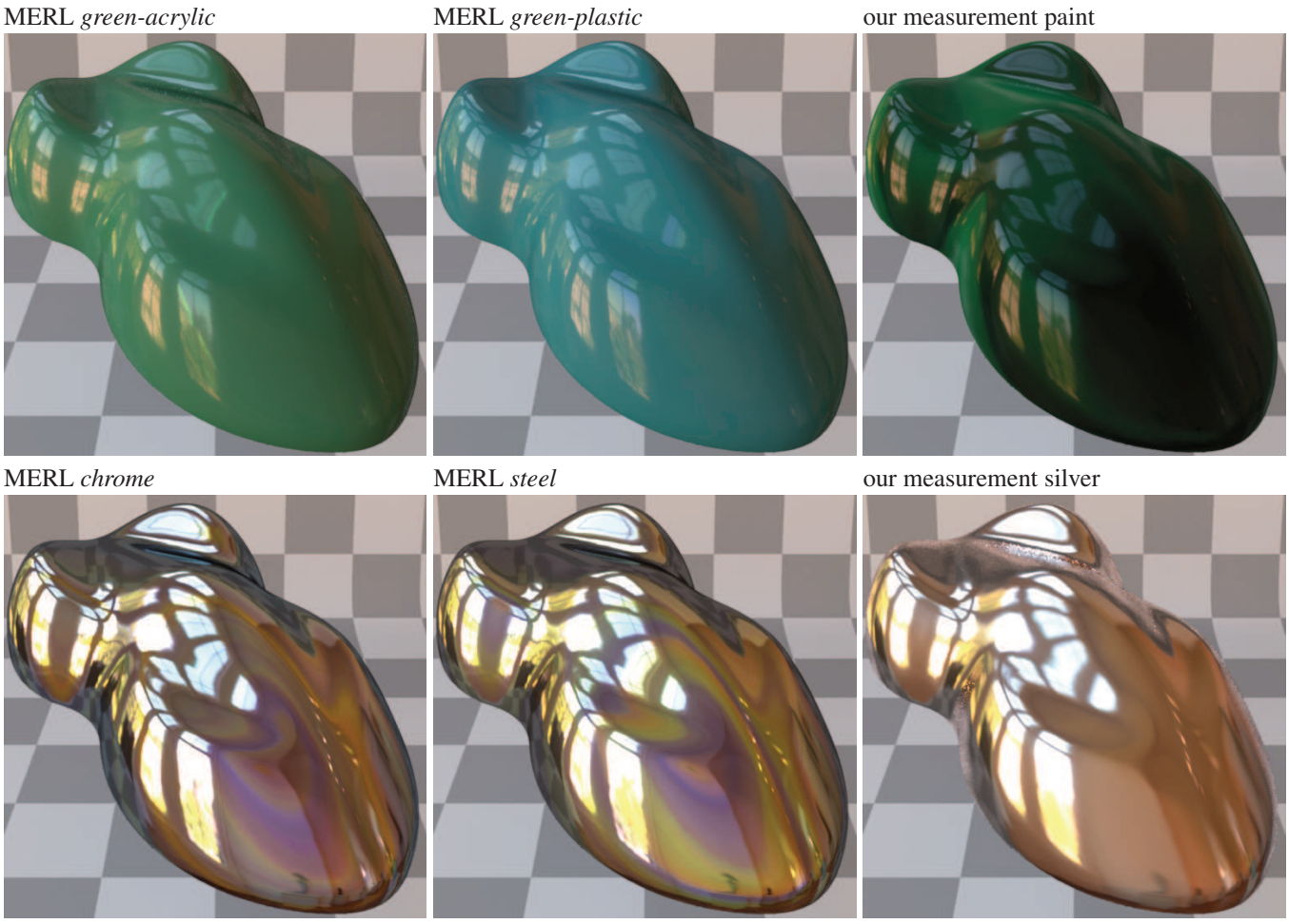


Figure 17: A comparison of ray-tracing of the captured BRDFs of paint and silver with similar materials from the MERL BRDF database using a Mitsuba renderer.

International Conference on Computer Vision. ICCV '95; Washington, DC, USA: IEEE Computer Society. ISBN 0-8186-7042-8; 1995, p. 80–.
[19] Ngan, A., Durand, F., Matusik, W.. Experimental analysis of BRDF models. Eurographics Symposium on Rendering 2005 2005;2:117–126.
[20] Filip, J., Vávra, R., Havlicek, M.. Effective acquisition of dense anisotropic BRDF. In: Proceedings of the 22th International Conference on Pattern Recognition, ICPR 2014. 2014, p. 2047–2052.
[21] Nicodemus, F., Richmond, J., Hsia, J., Ginsburg, I., Limperis, T.. Geometrical considerations and nomenclature for reflectance. NBS Monograph 160 1977;:1–52.
[22] Cook, R., Torrance, K.. A reflectance model for computer graphics. ACM SIGGRAPH 1981, ACM Press 1981;15(3):307–316.